

# Experiments on incipient channelization of submarine fans

## Expériences sur la formation de chenaux dans les deltas sous-marins

JASIM IMRAN, *Department of Civil and Environmental Engineering, University of South Carolina, Columbia, SC 29208, USA.*  
*imran@enr.sc.edu*

GARY PARKER and PETER HARFF, *Saint Anthony Falls Laboratory, Dept. of Civil Engineering, University of Minnesota, Minneapolis, MN 55414, USA.*

### ABSTRACT

Experiments on the formation of channelized submarine fans by the passage of successive turbidity currents are presented. Channels similar to subaerial rivers are found in many submarine fans. The inception of channels on submarine fans, which are essentially depositional environments, can be explained in terms of the lateral distribution of the rates of deposition and erosion of suspended sediment associated with a passing turbidity current. The experiments reported here supplement the findings of a numerical model developed earlier to study the inception of channel-levee systems on submarine fans. The experimental setup is a simple replication of a surface at the base of a continental slope receiving a turbidity current from a canyon. The turbidity current was generated by releasing a sediment-water mixture of low sediment concentration from an overhead tank into a quiescent water body held in a rectangular tank. The bottom slope of the tank was varied between 3 and 10%. Two sediment sizes, with geometric mean sizes of 71  $\mu\text{m}$  and 110  $\mu\text{m}$  were used. The bed profile was measured after the completion of each run. A 2-D depth-averaged numerical model of turbidity current was then run with the input conditions from the experiment. The resulting bed profiles were compared with the measured data. Generally good agreement between the experimental and numerical findings is observed.

### RÉSUMÉ

On présente des expériences sur des deltas sous-marins nervurés formés par le passage de courants de turbidité successifs. Des chenaux analogues aux rivières terrestres se trouvent dans beaucoup de deltas sous-marins. L'apparition de chenaux dans les deltas sous-marins, qui sont essentiellement des phénomènes de dépôt, peut être expliquée par la distribution latérale des vitesses de dépôt et d'érosion des sédiments en suspension associée au courants de turbidité en transit. Les expériences rapportées ici complètent les résultats d'un modèle numérique développé auparavant pour étudier la création de systèmes de levées en bordure des chenaux dans les deltas sous-marins. Le montage expérimental est une simple représentation d'une surface à la base d'une pente continentale recevant le courant turbide d'un canyon. Le courant turbide était généré par le lâcher d'un mélange eau-sédiment de faible concentration, depuis un réservoir amont, dans un volume d'eau tranquille contenu dans un bassin rectangulaire. On a fait varier la pente du fond de ce bassin entre 3 et 10%. Deux tailles de sédiments sont utilisées: 71  $\mu\text{m}$  et 110  $\mu\text{m}$ . On a relevé le profil du fond à la fin de chaque essai. On a ensuite exploité un modèle numérique 2D de courant de turbidité moyenné sur la profondeur, avec, en entrée, les données de l'expérience. Les profils du fond calculés ont été comparés aux données mesurées. On a observé, en général, un bon accord entre les résultats expérimentaux et numériques.

### 1. Introduction

A wide variety of geophysical and engineering flows can be classified as density currents. Examples include katabatic winds, dust storms, saltwater intrusions in estuaries, convective currents in lakes and reservoirs, hyperpycnal plumes caused by 'dirty' rivers flowing into the ocean, and dense vapor clouds emitted by industrial stacks (Turner, 1973; García, 1990; Tsihrintzis and Alavian, 1996; Simpson, 1997; Mulder and Syvitski, 1994). Turbidity current is a subset of density current that occurs in ocean and lake bottoms (Parker et al., 1986). The driving force of turbidity current is obtained from the particulate phase, i.e. suspended sediment, which renders the flowing turbid water heavier than the clear water above (Garcia, 1992). Submarine density current can also occur due to thermal stratification and salinity gradient. During the flow, a turbidity current can exchange sediment with the erodible bed by erosion and deposition. Turbidity currents often represent a hazard, which in appropriate conditions can place man's underwater activities at considerable risk (Hay, 1987a). Testimony to their destructive power and the potential damage to seabed structures are provided by instances of submarine cable breakage (e.g. Heezen and Ewing, 1952).

Turbidity currents traversing low slopes can be expected to be depositional in the gross sense, providing the mechanism for the formation of subaqueous fans. Many such fans, however, are not simply sheets of sediment deposited from turbidity currents, but instead show an intricate pattern of channelization. Examples of channelized fans include such large fans as the Amazon, Mississippi, Bengal, Indus, and Zaire. These channels form in an overall depositional environment and act as a conduit of sediment delivery to distances up to thousands of kilometers (e.g., Peakall et al., 2000). Figure 1(a) shows several meandering channels on the Amazon Submarine Fan. The submarine fan and the meandering channels obtained their sediment supply by turbidity current generated in the canyon. These channels are surrounded by high natural levees and have beds perched well above the elevation of the adjacent non-channelized regions [Figure 1(b)]. The issue of how channels can be maintained and elongated as they stack up in a depositional environment has remained largely unresolved.

Economic interest associated with valuable hydrocarbons reserves found in submarine fans and the intrinsic attractiveness of the fan morphology has generated considerable interest in the study of turbidity currents. Several conceptual models have been developed from both modern and ancient examples to characterize

Revision received January 29, 2001. Open for discussion till August 31, 2002.

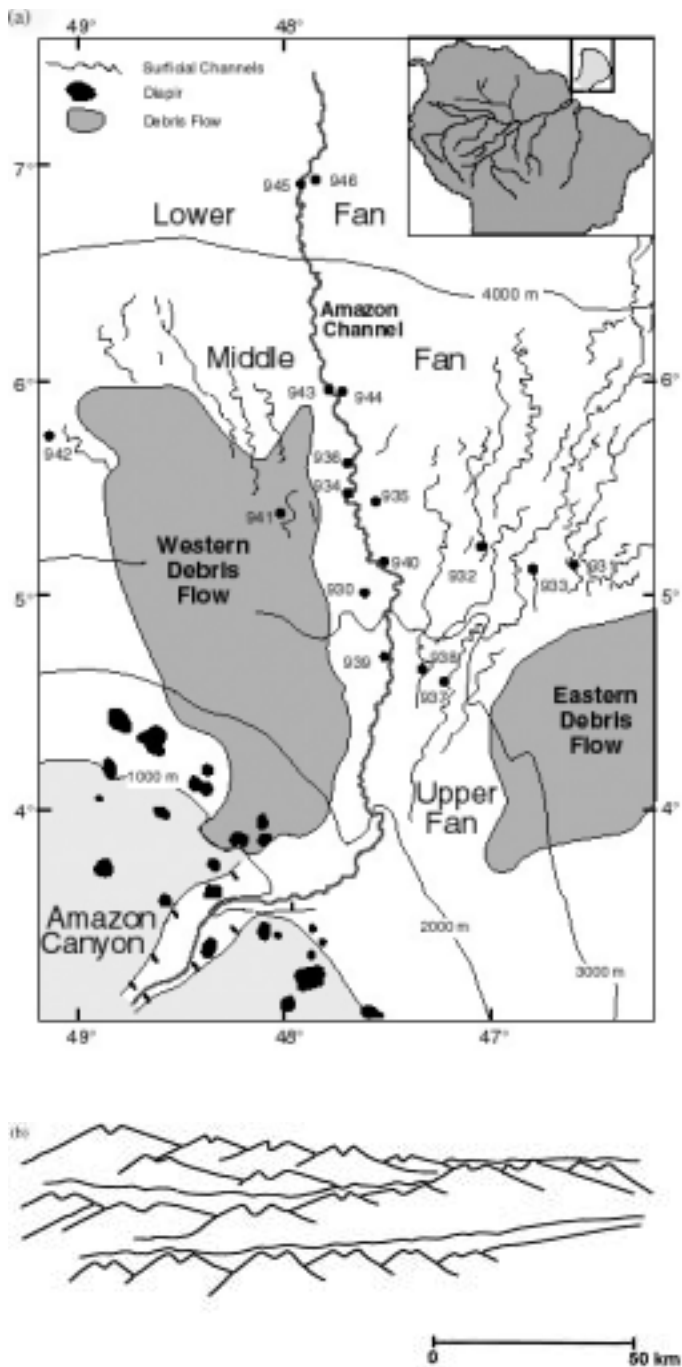


Fig. 1 (a) Bathymetric map of the Amazon Submarine Fan that shows a meandering channel extended several hundred kilometers from the Amazon Canyon. In addition to the youngest Amazon Channel, several abandoned channels can be also found. The numbered black dots are drilling locations where the Ocean drilling program collected sediment cores (Courtesy: Carlos Pirmez). (b) Cross-fan structure of the Amazon Submarine Fan showing channels perched well above the fan bed (Modified from Flood et al., 1991).

morphologies and patterns of facies distribution of submarine fans (e.g., Stow et al., 1985). Recent acoustic imaging techniques such as side-scan sonar have revealed the sedimentary features of several deep-sea fans in some detail (e.g., Twichell et al., 1991), and have encouraged further speculation as to the nature of fan formation. Existing descriptive models have not, however, re-

vealed the mechanics of the process of channelization on submarine fans. Hay (1982) envisaged that during a flow event, a turbidity current can maintain a core of high velocity which renders the lateral distribution of the rate of erosion of sediment into suspension tighter than that of the deposition rate. As described below, the process of channel inception can be explained by superimposing the distribution of the erosion and deposition rates in the lateral direction so as to determine the net rate of deposition (Imran et al., 1998).

There have been also numerous research efforts to understand the mechanics of density currents in general. Most of the experimental work on density currents flowing along inclined or horizontal boundaries has concentrated on the conservative case, for which the agent of the density difference is neither lost nor gained during flow; some examples are work of Ellison and Turner (1959), Simpson and Britter (1979) and Britter and Linden (1980). Turbidity currents are, however, intrinsically non-conservative in that sediment can be gained by erosion or lost by deposition. Some researchers have performed experimental studies of turbidity currents that are purely depositional (Middleton, 1967; Tesaker, 1969; Siegenthaler and Buhler, 1985; García, 1990, 1994), currents for which erosion and deposition occur simultaneously (García, 1990; García and Parker, 1991, 1993; Boncacez et al., 1993) and currents that are locally neither depositional nor erosional (Stefan, 1973; Ashida and Egashira, 1975). These experiments were two-dimensional, allowing variability in the streamwise and normal (to the bed) directions. Fietz and Wood (1967) and Tsihrintzis and Alavian (1996) performed experiments on three-dimensional spreading conservative currents. The experiment of Boncacez et al. (1995) involved an axisymmetric depositional current.

There are also several mechanistic models of turbidity currents that admit simultaneous deposition and erosion of sediment (e.g., Pantin, 1979; Lüthi, 1980; Parker, 1982; Fukushima et al., 1985; Parker et al., 1986; Hay, 1987a,b; Stacey and Bowen, 1988a,b; Eidsvik and Brørs, 1989; García, 1994; Takahata, 1995; Mulder et al., 1997; and Salaheldin et al., 2000). The above models, by not allowing variation in the lateral direction, do not reveal the causative mechanism for self-channelization of submarine fans. In order to describe the inception of a channel from a depositional turbidity current, variation of flow and deposit in the lateral direction must be allowed. This alone, however, does not guarantee the inception of a channel. The motivation of the present study is the observation of incipient spontaneous self-channelization within the deposit of a turbidity current.

Recent efforts by Imran et al. (1998) and Bradford (1996) were devoted to the development of a mechanistic model which can capture the lateral variation of both the turbidity current and the associated bed morphology of an evolving submarine fan. Imran et al. (1998) noted that the distribution profile of the deposition and erosion rates in the cross-stream direction during the flow of a turbidity current can explain the inception of any of the three basic types of submarine channels shown in Figure 2. For a specific sediment size, the erosion rate from bed into suspension  $E$  (volume of sediment eroded from the bed per unit bed area per unit time) can be expected to be proportional to the magnitude of

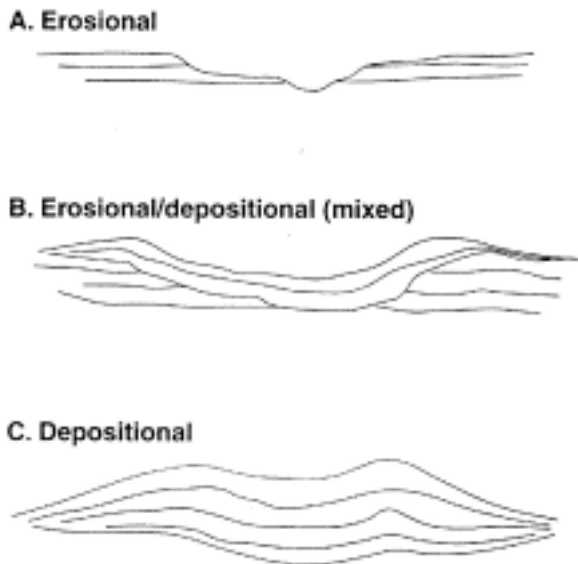


Fig. 2 Three basic types of submarine channels. From Clark and Pickering, 1998.

the bed shear stress to some power  $n$ , where  $n \approx 1$  (e.g. García and Parker, 1991). The magnitude of the boundary shear stress can in turn be assumed to depend on the square of the magnitude of the depth-averaged flow velocity vector  $|\bar{u}|$ . That is, for a given grain size, whereas the deposition rate  $D$  depends linearly on concentration  $C$ , the erosion rate depends on the magnitude of the velocity vector to a power that is at least 2. Since the flow itself is driven solely by the presence of sediment, the scaling  $D \sim C$  and  $E \sim |\bar{u}|^2$  suggest that the erosion rate  $E$  might be more peaky, i.e. decline more rapidly in the transverse direction than the deposition rate  $D$ , as shown in Figure 3. The net rate of deposition of sediment on the bed,  $D - E$  might then possess a minimum along the axis of the submarine canyon from which the current emerges, and a maximum on each side, eventually tapering off to zero far from the axis. This pattern of net deposition would delineate in-

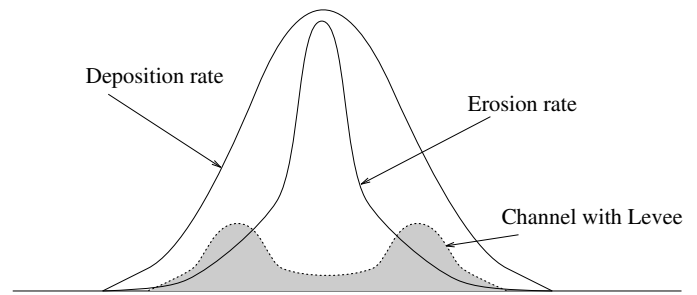


Fig. 3 Schematic description of lateral distributions of erosion and deposition rates the combination of which can explain the inception of a channel bounded by natural levees.

ipient natural levees bounding a channel. Even a flow environment that is overall depositional, i.e.  $E < D$  everywhere, can thus result in the spontaneous inception and subsequent buildup of a distinct channel-levee system, as shown in Figure 3. The theoretical basis of this argument can be found in the work of Imran et al. (1998). The hypothesis that the transverse variation of the erosion rate  $E$  has a more tight distribution than that of the deposition rate  $D$  is at the heart of this proposed mechanism of channelization. If however, the flow velocity is sufficiently low, so that the threshold for erosion is not exceeded, the deposit will be unchannelized (e.g., Alexander and Morris, 1994). Imran et al. (1998) developed a numerical model to explore this hypothesis. The model was used for identifying the relative effect of different flow parameters on the incipient tendency for the formation of fan channels. A regime of incipient channel formation in accord with the above description was successfully identified. Such a numerical model, no matter how carefully formulated, is almost impossible to test in the field. With this in mind, the study reported here was conducted to test the performance of the numerical model. The goal is to validate or disprove the numerical model findings both in terms of local predictions and overall behavior and morphology.

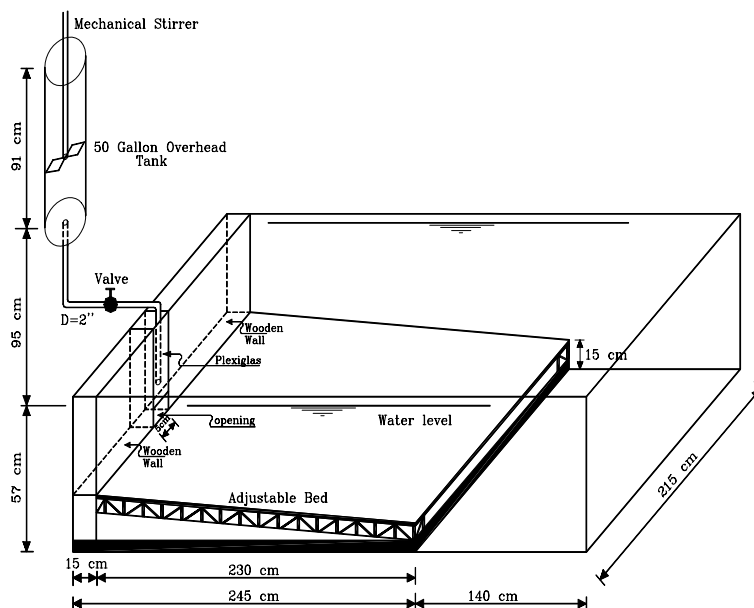


Fig. 4 A 3-D view of the experimental setup.

## 2. Experimental Setup and Procedure

The experimental setup is illustrated in Figure 4. Simplified though the experimental setup may be, the similarity with the natural setting of Figure 1 is readily apparent. The basin used in the experiments is a rectangular steel tank 3.75 m long, 2.15 m wide and 0.5 m deep filled with fresh water. A rectangular horizontal concrete slab 5 cm thick extends to a length of 2.25 m, beyond which the steel bottom of the tank is exposed. Above the slab is a steel platform of adjustable slope. This bed is 2.25 m long and 2.15 m wide, and is mounted on a frame. The canyon-fan transition occurring in nature is reduced here to a simple slot opening with a width of 15 cm centered along the upstream wall of the basin. A Plexiglas gate controls the opening. The opening is indented 15 cm upstream of the gate; the wooden walls on either side simulate canyon walls. The size of the opening can be reduced by means of adjustable blocks. In all the experimental runs the opening was set to be 8 cm high and 5 cm wide. The downfan distance  $x$  and the lateral distance  $y$  were measured from the upper right corner of the basin looking downstream (Figure 4). In analyzing the data, these distances are normalized by the inlet width  $b$  and the thickness of the deposit is normalized by inflow current thickness  $h_0$ . A pipe with a diameter of 5.08 cm (2 inches) brought the dilute suspension from a cylindrical 50-gallon overhead tank to the inlet gate of the basin.

In order to produce a turbidity current a suspension of fine sediment was created in the head tank by filling it with water, pouring in a specified amount of fine sediment and stirring with a mechanically operated propeller. When the sediment was thoroughly mixed with the water, a valve was opened so as to quickly deliver the sediment suspension through the submerged gate of the plexiglas-chamber into the basin. The turbidity currents so simulated were discrete in nature, with each current lasting about 20 seconds. Continuous currents were precluded by the setup of the basin, which did not allow for withdrawal of the current at the distal end, thus resulting in reflection of the turbidity current. The reflection produced by a continuous run would pollute the tank with sediment in a short period of time, and thus reduce the density difference between sediment-laden and clear water that drives the current. The setup thus placed both a lower bound on the size of sediment that could be successfully employed, and an upper bound on the duration of flow. The limitations resulting from these restrictions are discussed below.

A typical run consisted of 20 discrete events, each introducing approximately 94.6 liters (25 gallons) of water with a concentration of 2% suspended sediment by volume. Each event was separated by about five minutes (the time required to refill the head tank with water, introduce the sediment and mix the suspension). In cases where sediment pollution appeared to be excessive, more time was allowed between events. Sediment of two different sizes, namely 71  $\mu\text{m}$  and 110  $\mu\text{m}$  were used in the runs reported here mainly because these two grades were well sorted and contained very small quantities of fines. The great majority of the sediment settled out before it could reflect from the distal wall, thus reducing pollution of the ambient water of the basin. The sediments had a specific gravity of 2.65; the geometric standard

deviations of the 110  $\mu\text{m}$  and 71  $\mu\text{m}$  sediment were 1.125 and 1.25 respectively.

Turbidity currents were passed over an initially inerodible bed consisting of the steel platform spray-painted with 110  $\mu\text{m}$  sand to provide roughness. The inflow velocity was determined by recording the rate of drop of the water level in the head tank. A typical inflow velocity of the turbidity current for a surge is shown in Figure 5. The drop of head that gives the inflow momentum of the turbidity current between the beginning and end of a surge was 40 cm, approximately 20% of the total head. The velocity  $U$  scales as  $U \sim H^{1/2}$ , where  $H$  is the head difference between the overhead tank and the basin. As shown in Figure 5, even though the linear fit of velocity shows an overall decline with time, it is not larger than the fluctuation caused by the hand held stirrer. With this in mind, the characteristic inflow velocity for an event was taken to be the average value over 20 seconds. The inflow mean velocities for each surge event of the experimental runs used here as a basis for testing the numerical model are plotted in Figure 6. The mean surge velocities shown in that figure are fairly close to a constant value averaged over all surges for a given run. The latter can be used in the numerical simulation without loss of comparability.

The choice of 20 surge events per experiment was made in order to provide a deposit of sufficient thickness to observe whether incipient channelization resulted. At the end of an experiment the bed was measured with a point gauge without draining the overlying standing water, so as to avoid any disturbance. The runs for which complete documentation were obtained are summarized in Table 1.

## 3. Description of the Numerical Model

In this section the numerical model is described briefly. For de-

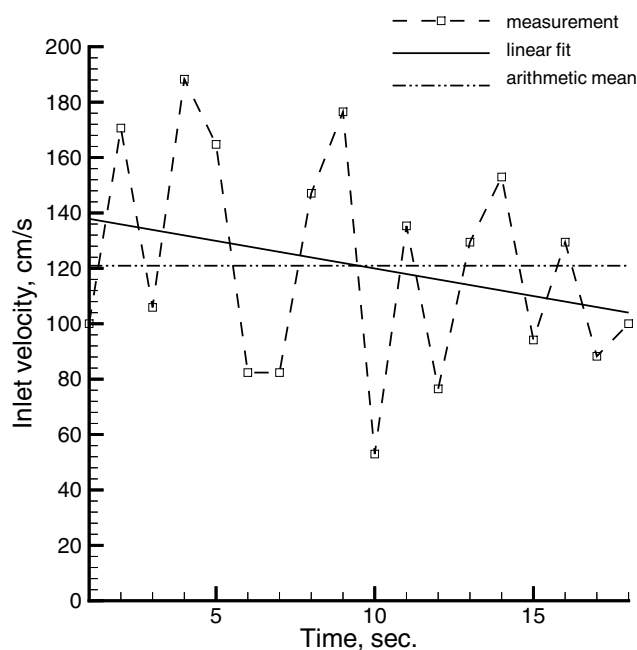


Fig. 5 Inlet velocity versus time for a typical release (surge no. 8 of run S6D71).

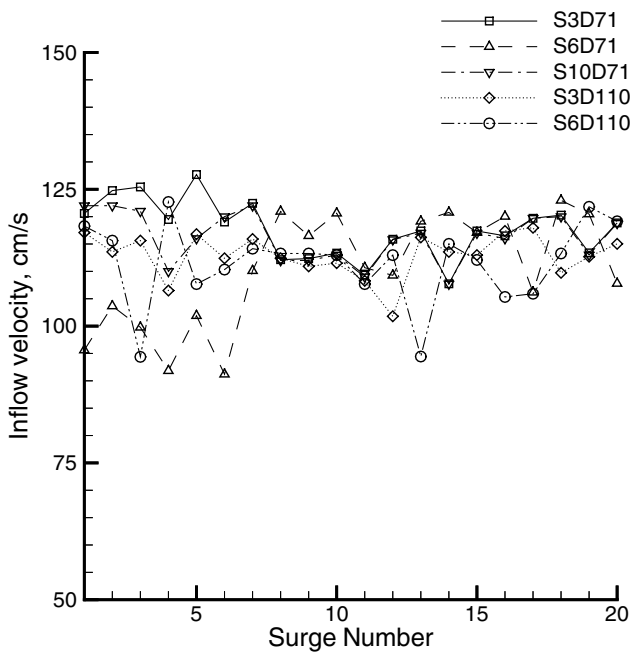


Fig. 6 Inflow velocity averaged over each surge for the runs listed in Table 2.1.

Table 1 Experimental conditions

RUN	$\bar{U}_0$	$C_0$	$D_s$ ( $\mu\text{m}$ )	Slope (%)	$h_0$ (cm)	$C_f$
S3D71	118	$2.0 \times 10^{-2}$	71	3	8	0.0035
S6D71	110	$2.0 \times 10^{-2}$	71	6	8	0.004
S10D71	117	$2.0 \times 10^{-2}$	71	10	8	0.0035
S3D110	112	$2.0 \times 10^{-2}$	110	3	8	0.008
S6D110	112	$2.0 \times 10^{-2}$	110	6	8	0.008

tails see Parker et al. (1986) and Imran et al. (1998). The numerical model consists of a set of layer-integrated equations describing the flow of a turbidity current and the Exner equation of sediment continuity, which describes the change of bed level driven by the exchange of sediment between the bed and the current. The flow model is essentially a two-dimensional extension of the one-dimensional model of Parker et al. (1986), the two-dimensionality allowing for the lateral spreading of suspended sediment and flow momentum. In addition to one conservation equation for water mass and two conservation equations for flow momentum (downslope and transverse), the conservation of mass of the suspended sediment is described as well. In the Exner equation of sediment continuity, the change of bed elevation is calculated by considering the erosion and deposition by suspended sediment only.

Both continuous and surge-type turbidity currents have been recognized in the field (e.g. Hay, 1987a,b). The numerical model can be run with either of these inflow boundary conditions. To simulate surge-type experiments the following procedure is adopted. At time  $t = 0$  the surface of the fan is inactive, but a current is commenced along a line corresponding to the rectangular inlet of the experimental basin. The surge front is allowed to propagate for 20 seconds, i.e. the duration of a surge in the experiment, during which time sediment is allowed to exchange freely with the

bed. The calculation is then halted, and recommenced after imposing the same initial conditions for all flow parameters except the bed, which is initialized at the final configuration of the previous surge. This procedure is repeated in the numerical calculation for the same number of surges as the experiment to be modeled. Since the main focus of this paper is the experiments, description of the governing equations and the solution technique are relegated to the Appendix.

#### 4. Numerical and Experimental Results

The measured bed profiles are compared with the results of the numerical simulation in this section. As mentioned earlier, two different sediment sizes and three different bed slopes were considered to study the effect of sediment size and initial bed slope on incipient fan channelization. In the previous numerical study by Imran et al. (1998), these two parameters were found to have particularly strong influences on the length and shape of an incipient channel. In order to simulate an experiment, the friction factor  $C_f$  described in the Appendix must be specified as an input parameter. Unlike open channel flow, standard resistance relations are not available for turbidity current. Therefore, the friction factor was obtained by calibration of the predicted deposit against the observed ones. The values so obtained are reported in Table 1. They are within the range commonly reported in the literature for experiments (e.g., Parker et al., 1986; García and Parker, 1993). The difference in calibrated friction factor between different runs deserves some discussion, which is presented later. Before discussing the results in detail, it is of value to have a brief first look at the experimentally and numerically obtained deposit profiles. In Figure 7, the experimental and numerical results for

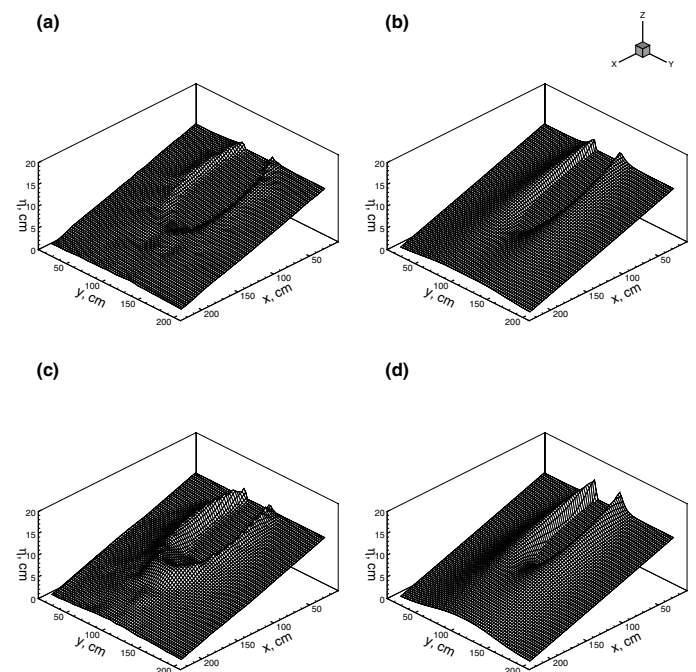


Fig. 7 3-D view of the sediment deposit; (a) S6D71 (measured); (b) S6D71 (simulated); (c) S6D110 (measured); (d) S6D110 (simulated).

runs S6D71 (initial slope = 6 %, grain size = 71  $\mu\text{m}$ ) and S6D110 (initial slope = 6 %, grain size = 110  $\mu\text{m}$ ) are compared. An overall similarity of pattern, with an incipient channel and levees extending from the inlet, is apparent. The zone of poorest agreement, however, is toward the distal end of the incipient channel. Comparison of measured and computed deposit thickness along several transects perpendicular to the incipient channel follows below.

The first set of direct comparisons is given in Figure 8, which is devoted to a study of the effect of varied initial slope on incipient channelization. That is, sediment size is held constant at 71  $\mu\text{m}$  but three initial slopes, 3, 6 and 10 percent are considered. Mean inlet velocity differs in the experiments, but only modestly. Measured and computed deposit thickness for runs S3D71, S6D71 and S10D71 are compared along 8 transverse transects taken at different downfan distances from the inlet. In the plots downfan distance  $x$  and the transverse distance  $y$  are normalized against inlet width  $b$ , which is equal to 5 cm in all experiments reported here. Likewise the deposit thickness  $\eta$  is normalized by the in-

flow current thickness  $h_0$ , which was set equal to 8 cm for all of the runs. The second set of comparisons is given in Figure 9, which provides an additional study of the effect of varied initial slope on incipient channelization, this time for 110  $\mu\text{m}$  material. The two slopes studied are 3 % (run S3D110) and 6 % (run S6D110), again using 8 transverse transects of deposit thickness. The third set of comparisons, given in Figure 10, allows for a study of the effect of changing grain size at the same slope; the runs in question are run S6D71 and S6D110, so that the initial bed slope is 6% and the grain sizes are 71  $\mu\text{m}$  and 110  $\mu\text{m}$ . The results are presented in terms of 8 transverse transects.

Neither Figure 8 nor Figure 9 indicates a strong dependence of computed channel cross-sectional shape on slope over the range studied. The only major deviation appears in the distal transects ( $x/b = 26$ ) toward the end of the channel where the channel tends to be narrower and levees tend to be higher at lower slope. The experimental data exhibit a somewhat stronger variation with slope, with the proximal levees being lowest for the highest slope. The same trend continues to the distal zone for experiments with the smaller grain size. For experiments with larger grain size, however, in the distal zone, the measured deposit thickness is

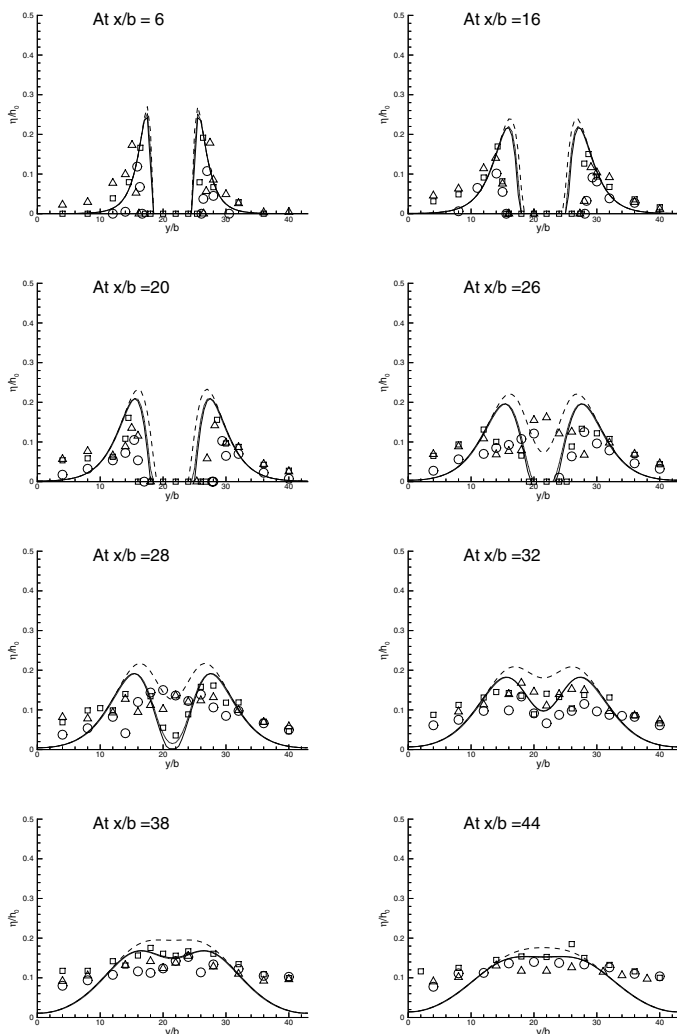


Fig. 8 Comparison of deposit thickness for runs performed with 71  $\mu\text{m}$  sediment. Run S3D71: triangle (experiment), dashed lines (simulation); Run S6D71: square (experiment); solid line (simulation); Run S10D71: circle (experiment), dotted lines (simulation).

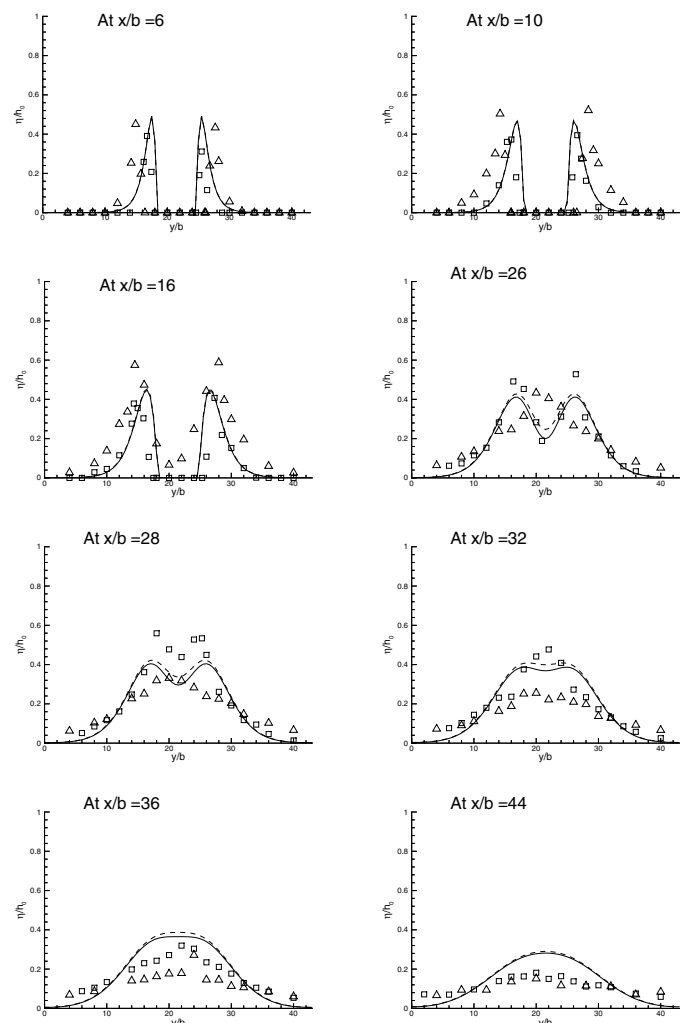


Fig. 9 Comparison of deposit thickness for runs performed with 110  $\mu\text{m}$  sediment. Run S3D110: triangle (experiment), dashed lines (simulation); Run S6D110: square (experiment); solid line (simulation).

smaller at lower slope, a trend that is contrary to the numerical findings (Figure 9). The downchannel distance below which the channel starts to lose definition is relatively shorter at the lowest slope (3%) from both experiments and simulation. In general the effect of initial bed slope on the deposition profile is more pronounced for experiments with larger grain size.

There is significant progressive increase with downstream distance in deposit thickness near the two lateral boundaries in all the experiments. The numerical simulation shows a similar trend but with smaller deposition near the boundaries. Although the agreement between the experimental measurement and the simulation are reasonably good in the middle half of the domain width, near the lateral boundaries, where the deposits are thinnest the experimental and simulated profiles do not agree very well.

The effect of grain size on the deposition profile is clearly demonstrated in Figure 10. An increase of sediment size from 71  $\mu\text{m}$  to 110  $\mu\text{m}$  has almost doubled the levee height, made the channel narrower and shortened the channel length by approximately 20 cm. While a channel-like depression continued near the end of the domain in run S6D71, the channel ended abruptly in run S6D110 shortly after the central region of the domain began to be covered

with sediment. The trends of both experiments were quite well reflected in their respective simulations.

As mentioned earlier, a calibrated constant friction factor was used in the numerical simulations. The friction factor or drag coefficient depends on the flow field, bed roughness and form drag exerted by bedforms. In analyzing their 2-D data, García and Parker (1993) separated the drag coefficient into two parts; one associated with the skin friction and the other related to the form drag (Nelson and Smith, 1989). They found from their measurements that form drag was typically larger than the skin friction. In the present three-dimensional study where bed elevation varied significantly in time and space, use of a constant friction factor grossly averages the effect of drag. The friction factor evaluated experimentally by García and Parker ranged from 0.02 to 0.08, and pertained to a much slower flow where a major portion of the resistance was contributed by the form drag. For model application, Parker et al. (1986) estimated a value of  $C_f = 0.004$  to be typical for field cases, based on a perusal of the literature (Komar, 1977; Inman et al., 1976; Shepard and Dill, 1966). In the present study, the friction factor was calibrated by running the numerical model with different values of  $C_f$  for two of the experimental runs S6D71 and S6D110 which used same initial bottom slope but different grain sizes. It was found that values of 0.004 and 0.008 respectively gave overall good match in levee height and channel length for these two runs. Both of these values are within the commonly cited range of 0.004 to 0.02 (e.g., Fukushima et al., 1985). The larger value of  $C_f$  for experimental run S6D110 may be attributed to the more rapid deposition and thus higher form drag associated with a thicker sediment deposit. The calibrated value of  $C_f = 0.008$  was used in simulating run S3D110. Runs S3D71 and S10D71 had a slightly larger inflow velocity compared to run s6D71 and therefore, a friction factor of 0.0035 which is slightly smaller than the calibrated value of 0.004 was deemed appropriate for these two runs.

## 5. Observations of Bedforms

Bedforms are common in many submarine deposits. The imaging of many deep-sea fans by side-scan sonar systems in the last decade has shown that coarse fan-valley and lobe sediments have a variety of large-scale depositional bedforms; regular sediment waves are also found to be developed in predominantly fine-grained sediments, principally on levees (Normark and Piper, 1991). Figure 11 shows large gravel waves on the Grand Banks deposits, mud waves on Monterey and Var Fans (Normark and Piper, 1991), and Barchan dune like features on levees of two main channels on the Ruhuhu delta in Lake Malawi, Africa (Johnson et al., 1995). García (1990) documented two-dimensional bedforms generated by passage of a dense saline bottom current over an erodible bed of crushed coal. In the present study, bedforms were observed to develop from the very beginning of all the experiments and continued to grow with successive surges. These bedforms formed on the outer side of the levees and at the end of the channel. This can be associated with flow that spreads like a sheet in a net depositional environment. Bedforms generated in one of the experimental runs (S6D71) are presented in

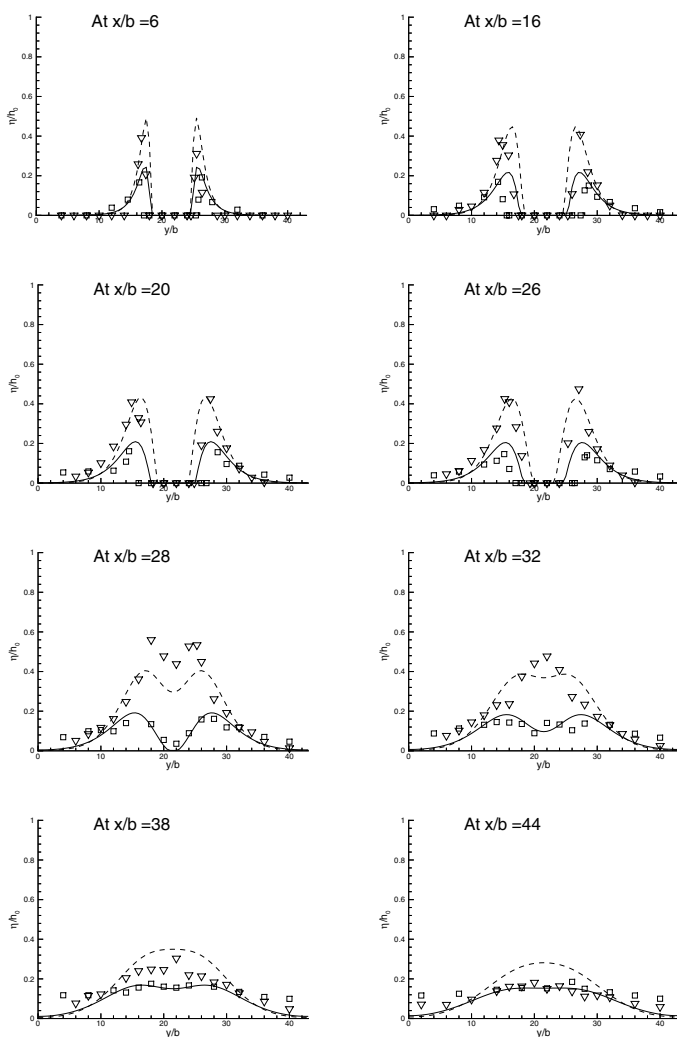


Fig. 10 Effect of sediment size on the bed profile. Run S3D71: gradient (experiment), dashed lines (simulation); Run S6D71: square (experiment); solid line (simulation).

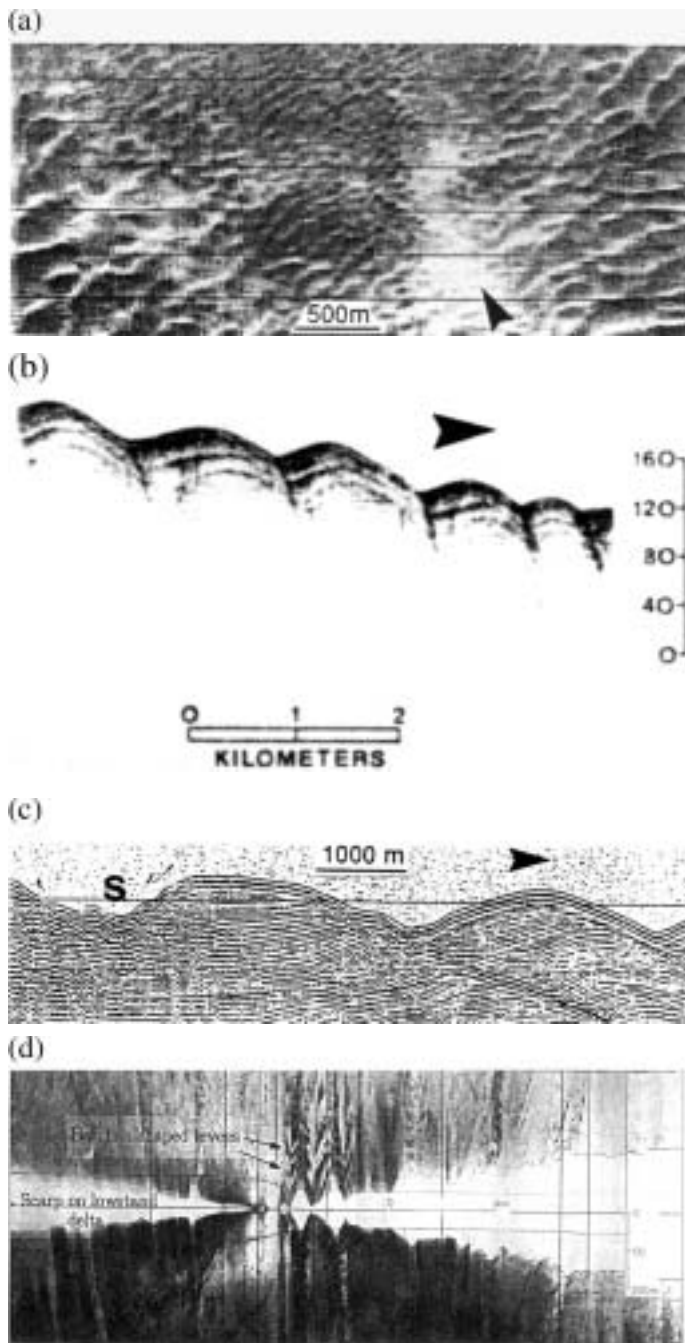


Fig. 11 Field examples of bedforms generated on turbidity current deposits: (a) Gravel waves on Grand Banks Turbidite; (b) Mud waves on Monterey Fan; (c) Mud waves on Var Fan; (d) Barchan dune like features on the levees of Ruhuhu Delta.

Figure 12, which shows the overall sediment deposit at the end of the run and a close-up of the detailed structure on the outside of a levee. The numerical model, with its depth-integrated formulation is not capable of capturing the mechanism of bedform formation.

## 6. Summary and Conclusions

As can be seen from Figure 7, the numerical model predicts incipient channel forms on a model submarine fan that are quite similar to the ones obtained via experimentation. The ability of the

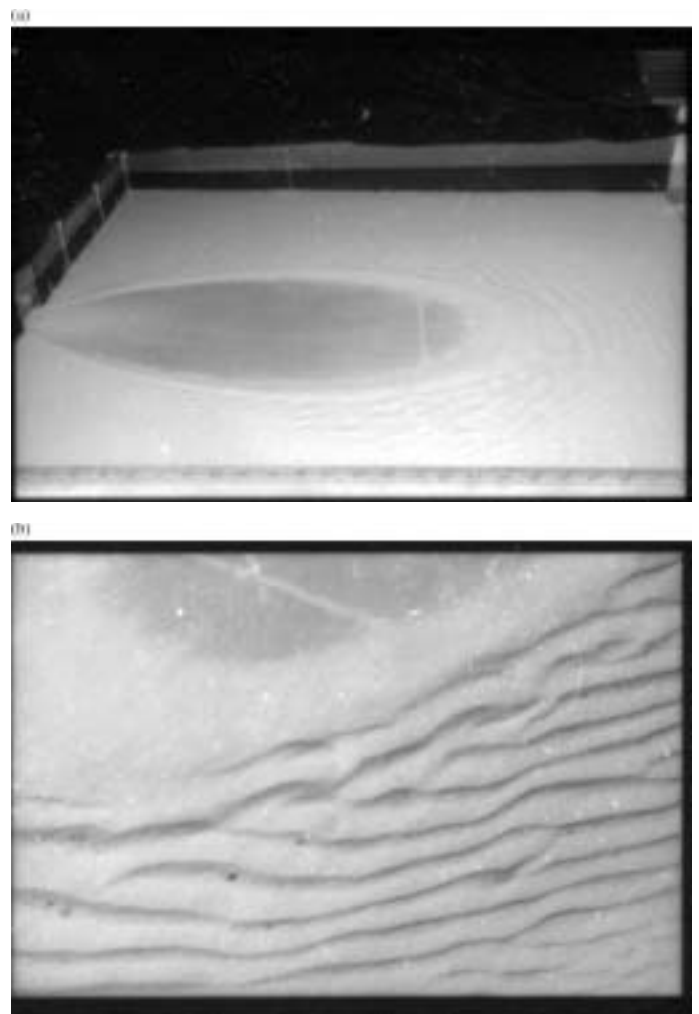


Fig. 12 Image of bedform generated in the experiment: (a) Overall view of the sediment deposit at the completion of run S6D71; (b) A closeup view on the backside of a levee from the same run.

model to provide adequate predictions at this small experimental scale lends credence to its application at field scale. Most of the submarine fans that have been surveyed represent systems with fully developed channels. The fact that limitations of the experimental facility and the numerical model used in the current study allow simulation of only incipient channels makes it difficult to make even a qualitative comparison with fully developed channels. However, a recently acquired acoustic image of a submarine sediment deposit (personal communication with Dan Orange, University of California, Santa Cruz) at the base of the Cascadia Margin between the latitudes of  $41^{\circ}$  N and  $41^{\circ} 30'$  N (Figure 13) shows remarkable qualitative similarity with the numerical results of Imran et al. (1998) and the present experimental study. Although this geomorphic feature is yet to be studied and interpreted in detail, preliminary observation suggests that it may be a young submarine fan either in the process of formation or arrested before complete formation. The channels on the continental slope visible in the image act like a drainage basin, supplying the sediment to the fan as turbidity current. An incipient channel on the fan at the end of the feeder canyon is clearly visible. These positive comments notwithstanding, several limitations of the work deserve scrutiny. The model basin was quite small, with

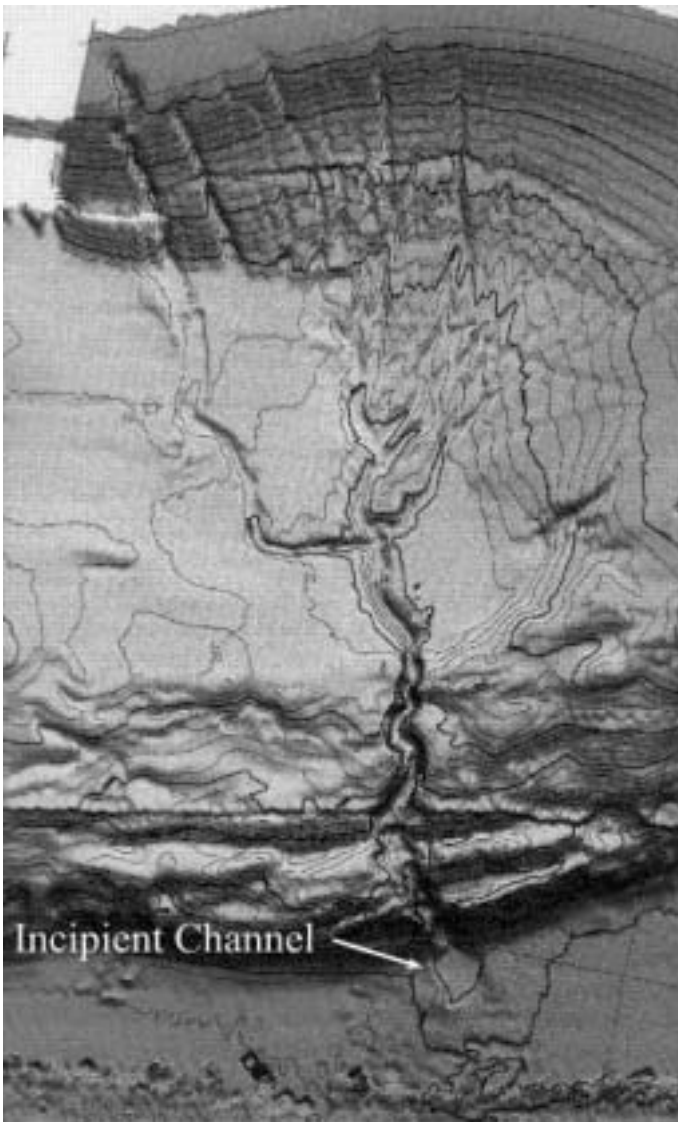


Fig. 13 An acoustic image of the Cascadia margin approximately between latitudes 41 ° N, 125 ° W and 41 ° 30' N, 124 ° W shows incipient channelization at the base of the continental slope. The fan receives sediment supply from a network of erosional channels acting like a drainage basin (Courtesy Daniel Orange, University of California, Santa Cruz)

a length of only 2.25 m. In addition, no mechanism was provided for the turbidity current to be vented at the downstream end. Sufficiently fine-grained turbidity currents were found to reflect off the back wall of the tank, sending a return wave of sediment-laden water and polluting the ambient water and disturbing the deposit. It was thus necessary to use sediment sizes so coarse (relative to the scale of the flow) as to ensure nearly complete settling before the turbidity current reached the end of the tank. This in turn necessitated the use of high inlet velocities of 1 m/s or more to maintain the sediment in suspension for at least some distance. Inlet bulk densimetric Froude numbers were as high as 7.2, indicating that the flow was entering into the basin like jets instead of negatively buoyant plumes.

These limitations in themselves pose no intrinsic problem for the numerical model, which should be applicable to the conditions of the experimental basin. They do, however, suggest that the re-

gime of channelization observed in the experiments may be somewhat different from the regime under which channelization occurs on submarine fans. This is likely reflected in the fact that initial bed slope, which was found to be an important parameter for channelization under the conditions studied by Imran et al. (1998), played little role in either the experiments or the numerical calculations reported here.

In an experimental facility more typical of field conditions, the tank would be much longer and a provision would be made at the downstream end for removing the turbidity current by e.g. siphoning without reflection. In such a configuration it would be possible to run continuous turbidity currents carrying finer material, with more plume-like rather than jet-like conditions at the inlet. Another cause of some discrepancy may have been the neglect of bedload in the numerical model. While turbidity currents are by definition driven by suspended load, they are capable of transporting sediment as bedload as well. The bedforms observed in the course of the present experiments appeared to be at least partly controlled by bedload. The form drag associated with the bedforms suggests that the assumption of spatially constant friction factor  $C_f$  used in the numerical model is a fairly crude approximation.

Perhaps the most consistent discrepancy between the experimental and numerical results is the tendency for the experimental deposits to be thicker near the side walls of the tank than those predicted numerically. Since the deposits are thin in both cases, the point might not be considered too critical. It nevertheless suggests that the transverse diffusion or dispersion of sediment by turbulence, which is neglected in the numerical model, may be playing a role in determining morphology. This limitation may be overcome by employing a version of a depth-integrated turbulence model (e.g.  $k-\epsilon$ ) adapted to turbid underflows.

## Appendix I: Governing Equations and Solution Technique

The governing equations of a turbidity current and the associated exchange of sediment between the bed and the current are given below in vectorial form. For simplicity only material with a uniform grain size is considered here. In addition, the Coriolis acceleration may be neglected at the experimental scales studied here.

$$\frac{\partial \mathbf{U}}{\partial t} + \frac{\partial \mathbf{F}}{\partial x} + \frac{\partial \mathbf{G}}{\partial y} + \mathbf{S} = 0 \quad (1)$$

where

$$\mathbf{U} = \begin{bmatrix} h \\ uh \\ vh \\ Ch \end{bmatrix} \quad (2a)$$

$$\mathbf{F} = \begin{bmatrix} uh \\ u^2h + \frac{1}{2}RCgh^2 \\ uvh \\ uCh \end{bmatrix} \quad (2b)$$

$$\mathbf{G} = \begin{bmatrix} vh \\ uvh \\ v^2h + \frac{1}{2}RCgh^2 \\ vCh \end{bmatrix} \quad (2c)$$

$$\mathbf{S} = \begin{bmatrix} -e_w (u^2 + v^2)^{\frac{1}{2}} \\ RCgh \frac{\partial \eta}{\partial x} + C_f (u^2 + v^2)^{\frac{1}{2}} u \\ RCgh \frac{\partial \eta}{\partial y} + C_f (u^2 + v^2)^{\frac{1}{2}} v \\ D - E \end{bmatrix} \quad (2d)$$

The Exner equation for sediment continuity can be written as

$$(1 - \lambda) \frac{\partial \eta}{\partial t} = D - E \quad (3)$$

In the above equations  $x$  denotes a downslope coordinate starting at the upstream end,  $y$  is a transverse coordinate,  $t$  is time,  $h$  is current thickness normal to the bed,  $u$  and  $v$  are layer-averaged flow velocities in the  $x$  and  $y$  directions respectively,  $e_w$  is a coefficient of entrainment of sediment-free water from above into the turbidity current,  $C_f$  is dimensionless friction factor given by

$$\tau_b = \rho C_f (u^2 + v^2) \quad (4)$$

where  $\tau_b$  denotes the magnitude of the bed shear stress vector,  $\rho$  denotes water density,  $g$  denotes the acceleration of gravity,  $C$  denotes the volume concentration of suspended sediment in the flow,  $D$  and  $E$  denote the rates of deposition from and erosion into suspension, respectively, in volume per unit bed area per unit time,  $R$  denotes the submerged specific gravity of sediment, given by  $(\rho_s/\rho - 1)$  where  $\rho_s$  denotes sediment density, and the parameter  $\eta$  denotes the bed level. Internal relations are required in order to close the problem. Here the friction factor  $C_f$  is simply assumed to be a prescribed constant. The coefficient of water entrainment  $e_w$  is specified using the relation given by Parker et al. (1986);

$$e_w = \frac{0.00153}{0.0204 + Ri} \quad (5)$$

where  $Ri$  is the bulk Richardson number, given by

$$Ri = \frac{RCgh}{u^2 + v^2} \quad (6)$$

The deposition rate is specified in terms of settling velocity of the sediment and the near-bed concentration of suspended sediment  $c_b$ . Neither hindered settling nor the formation of flocs is considered in this simple analysis. The near-bed concentration  $c_b$  is related to the layer-averaged value  $C$  by a multiplicative constant  $r_0$ . In principle  $r_0$  should be a function of grain size, but here it is

set equal to the constant value of 2.0 in accordance with the experimental evidence of García (1990). Thus

$$D_s = v_s r_0 C \quad (7)$$

The fall velocity  $v_s$  is calculated using the relationship of Dietrich (1982). The relation for the erosion rate of bed sediment is taken to be that of García and Parker (1991), but modified for fine or light sediments using the results of García and Parker (1993). The modified relation takes the form

$$E = E_s v_s = a \frac{Z^5}{1 + \frac{a}{0.3} Z^5} v_s \quad (8)$$

where  $a$  is a constant having a value of  $1.3 \times 10^{-7}$  and

$$Z = \alpha_1 \frac{u^*}{v_s} R_p^{\alpha_2} \quad (9)$$

In the above relation,  $u^* = \sqrt{\tau_b / \rho}$  is the shear velocity, the parameters  $(\alpha_1, \alpha_2)$  take the respective values  $(1, 0.6)$  for  $R_p > 2.36$  and  $(0.586, 1.23)$  for  $R_p \leq 2.36$ , where  $R_p = \sqrt{RgD_s^3} / \nu$  is the particle Reynolds number, and  $D_s$  is the particle diameter. The modification in the sediment entrainment relation presented here from the original relation of García and Parker (1991) consists of the modified values of  $\alpha_1$  and  $\alpha_2$  for low values  $R_p$  implied by the results of García and Parker (1993). The above governing equations and the internal relations are non-dimensionalized as follows.

$$\begin{aligned} \hat{x} &= x/b, \quad \hat{y} = y/b, \quad \hat{h} = h/h_0 \\ \hat{u} &= u/U_0, \quad \hat{v} = v/U_0, \quad \hat{v}_s = v_s/U_0 \\ \hat{\eta} &= \eta/h_0, \quad \hat{C} = C/C_0, \quad \hat{t} = t/(b/U_0) \end{aligned} \quad (10)$$

Here  $b$  denotes the width of the canyon mouth and  $U_0$ ,  $h_0$  and  $C_0$  denote the values of  $u$ ,  $h$  and  $C$  at the canyon mouth. Non-dimensionalization allows for the interpretation of the numerical results at arbitrary scale. It also serves to delineate the dimensionless parameters that govern the problem. After non-dimensionalization, Equation 2 is solved by using the Beam and Warming implicit finite difference scheme (e.g., Fennema and Chaudhry, 1989) and Equation 3 is solved explicitly for each time step. For details see Imran et al. (1998).

## Appendix II: Notations

$b$	width of the simulated canyon mouth
$C$	depth-averaged volumetric sediment concentration
$C_0$	volumetric inflow sediment concentration
$C_b$	near-bed volumetric sediment concentration
$C_f$	drag coefficient
$D$	sediment deposition rate, volume per unit time per unit area
$D_s$	particle diameter
$E$	sediment erosion rate, volume per unit time per unit area
$E_s$	non-dimensional sediment erosion rate

$e_w$	non-dimensional entrainment rate of water into turbidity current column
$g$	acceleration due to gravity
$h_0$	height of the simulated canyon mouth
$r_0$	ratio of near bed and depth-averaged suspended sediment concentration
$R$	reduced specific gravity of sediment particles due to buoyancy
$Ri$	Richardson number
$R_p$	particle Reynolds number
$t$	time
$ \bar{u} $	magnitude of the depth-averaged velocity vector
$U_0$	inflow velocity at the simulated canyon mouth
$u^*$	shear velocity
$v_s$	fall velocity of the suspended sediment
$x$	streamwise distance from the upstream end
$y$	lateral distance from the upper right corner looking downstream
$u, v$	depth-averaged velocity in x and y directions respectively
$\eta$	bed elevation
$\tau_b$	bottom shear stress
$\lambda$	bed porosity
$\rho_s$	density of sediment particles
$\rho$	density of water.

## References

- ALEXANDER, J., and MORRIS, S. (1994), Observation on experimental, nonchannelized high-concentration turbidity currents and variations in deposits around obstacles. *J. Sed. Res.*, A64(4), 899-909.
- ASHIDA, K., and EGASHIRA, S. (1975), Basic study of turbidity currents. *Proc. JSCE*, 237, 37-50.
- BONECAZE, R.T., HUPPERT, H.E., and LISTER, J.R. (1993), Particle driven gravity currents. *J. Fluid Mech.* 250, 339-369.
- BONECAZE, R.T., HALLWORTH, M., HUPPERT, H.E., and LISTER J.R. (1995), Axisymmetric particle-driven gravity currents *J. Fluid Mech.* 294, 93-121.
- BRADFORD, S.F. (1996), Numerical modeling of turbidity current hydrodynamics and sedimentation, PhD dissertation, Univ. of Mich., Ann Arbor.
- BRITTER, R.E., and LINDEN, P.F. (1980), The motion of the front of a gravity current traveling down an incline. *J. Fluid Mech.* 99, 531-543.
- DIETRICH, E.W. (1982), Settling velocity of natural particles, *Water Resources Res.*, 18(6), 1615-1626.
- EIDSVIK, K.J., and BRØRS, B. (1989), Self-accelerated turbidity current prediction based upon  $k$ - $\epsilon$  turbulence. *Cont. Shelf Res.*, 9(7), 617-627.
- ELLISON, T.H., and TURNER, J.S. (1959), Turbulent entrainment in stratified flows. *J. Fluid Mech.* 6, 423-448.
- FEITZ, T.R., and WOOD, I.R. (1967), Three dimensional density current. *J. Hyd. Div.*, ASCE, 93(HY6), 1-23.
- FENNEMA, R.J., and CHAUDHRY, M.H. (1989), Implicit methods for two-dimensional unsteady free-surface flows, *J. Hyd. Res.* 27(3), 321-332.
- FUKUSHIMA, Y., PARKER, G. and PANTIN, H.M. (1985), Prediction of ignitive turbidity currents in Scripps submarine canyon. *Mar. Geol.*, 67, 55-81.
- GARCÍA, M. (1990), Depositing and eroding turbidity sediment-driven flows: Turbidity currents. Proj. Rep. 306, St. Anthony Falls Hydraul. Lab., Univ. of Minn., Minneapolis.
- GARCÍA, M. (1992), Turbidity currents. *Encyclopedia of Earth Sc.*, 4, 399-407.
- GARCÍA, M. (1994), Depositional turbidity current laden with poorly sorted sediment. *J. Hyd Eng.* 120(11), 1240-1263, 1994.
- GARCÍA, M., and PARKER, G. (1991), Experiment of bed sediment into suspension. *J. Hyd Eng.* 117(4), 414-435.
- GARCÍA, M., and PARKER, G. (1993), Experiments on the entrainment of the sediment into suspension by a dense bottom current. *J. Geophys. Res.* 98(c3), 4793-4807.
- HAY, A.E., (1982), The effects of submarine channels on river tailings disposal, In: *Marine Tailings Disposal*, pp. 139-181, Butterworth-Heinemann, Newton, Mass.
- HAY, A.E. (1987a), Turbidity currents and submarine channel formation in Rupert Inlet, British Columbia, 1. Surge observations. *J. Geophys. Res.* 92(c3), 2875-2881.
- HAY, A.E. (1987b) Turbidity currents and submarine channel formation in Rupert Inlet, British Columbia, 2. The roles of continuous and surge type flow. *J. Geophys. Res.* 92(c3), 2883-2900.
- HEEZEN, B.C., and EWING, M. (1952), Turbidity currents and submarine slumps, and the 1929 Grand Banks earthquake. *Am. J. Science.* 250, 849-873.
- IMRAN, J., PARKER, G., and KATOPODES, N. (1998) A numerical model of channel inception on submarine fans *J. Geophys. Res.* 103(C1), 1219-1238.
- INMAN, D., NORDSTROM, C.E., and FLICK, R.E. (1976), Currents in submarine canyons: an air-sea-land interaction. *Ann. Rev. Fluid Mech.*, 8, 275-310.
- JOHNSON, T., WELLS, J., and SCHOLZ, C.A. (1995), Deltaic sedimentation in a modern rift lake. *GSA Bull.*, 107(7), 812-829.
- KOMAR, P.D. (1977), Computer simulation of turbidity current flow and the study of deep-sea channels and fan-sedimentation. In *The Sea: Ideas and Observations in Progress in the Study of the Sea*, Vol. 6, Chap 15, (edited by E.D. Goldberg, I.N. McCave, J.J. O'Brien and J.H. Steel), Wiley.
- LÜTHI, S. (1980), Some new aspects of two-dimensional turbidity currents. *Sedimentology*, 28, 97-105.
- MIDDLETON, G.V. (1967), Experiments on density and turbidity currents, III. Deposition of sediment. *Can. J. Earth Sc.*, 4, 297-307.
- MULDER, T., and SYVITSKI, J. (1994), Turbidity currents generated at river mouths during exceptional discharges to world oceans. *J. Geol.*, 103 285-299.
- MULDER, T., SAVOYE, P., and SYVITSKI, J. (1997), Numerical modeling of a mid-sized gravity flow: the 1979 Nice turbidity current (dynamics, process, sediment budget and seafloor impact), *Sedimentology*, 44(2), 305-326.
- NELSON, J. M., and SMITH, J.D. (1989), Flow in meandering

- channels with natural topography. In: *River meandering*, S. Ikeda and G. Parker Eds., Water Resources Monograph No. 12, AGU, pp. 69-102.
- NORMARK, W.R., and PIPER, D.J.W. (1991), Initiation processes and flow evolution of turbidity currents: Implications for the depositional record. In *From Shoreline to Abyss: Contributions in Marine Geology in Honor of Francis Parker Shepard*, pp. 207-230, *SEPM Spec. Pub.*, 46, Tulsa, OK.
- PANTIN, H.M. (1979), Interaction between velocity and effective density in turbidity flow phase-plane analysis, with criteria for autosuspension, *Mar. Geol.*, 31, 59-99.
- PARKER, G. (1982), Conditions for the ignition of catastrophically erosive turbidity currents. *Mar. Geol.*, 46, 307-327.
- PARKER, G., FUKUSHIMA, Y. and PANTIN, H.M. (1986), Self-accelerating turbidity currents. *J. Fluid Mech.* 171, 145-181.
- PEAKALL, J., McCAFFREY, B., and KNELLER, B. (2000), A process model for the evolution, morphology, and architecture of sinuous submarine channels. *J. Sed. Res.* 70(3), 434-448.
- SALAHELDIN, T.M., IMRAN, J., CHAUDHRY, M.H., and REED, C. (2000), Role of fine-grained sediment in turbidity current flow dynamics and resulting deposits. *Mar. Geol.* 171 (1-4), 21-38.
- SHEPARD, F.P., and DILL, R.F., (1966), *Submarine Canyons and Other Sea Valleys*. Rand McNally.
- SIEGENTHALER, C., and BUHLER, J. (1985), The kinematics of turbulent suspension currents (turbidity currents) on inclined boundaries. *Mar. Geol.*, 64, 19-40.
- SIMPSON, J.E. (1997), *Gravity Currents in the Environment and the Laboratory (2nd ed.)*. Cambridge University Press, 244 p.
- SIMPSON, J.E., and BRITTER, R.E. (1979), The dynamics of the head of a gravity current advancing over a horizontal surface. *J. Fluid Mech.* 94, 477-495.
- STACEY, M.W., and BOWEN, A.J. (1988a), The vertical structure of density and turbidity currents: Theory and observations. *J. Geophys. Res.* 93(C4), 3528-3542.
- STACEY, M.W., and BOWEN, A.J. (1988b), The vertical structure of density and turbidity currents and a necessary condition for self-maintenance. *J. Geophys. Res.* 93(C4), 3543-3553.
- STEFAN, H. (1973), High concentration turbidity currents in reservoirs. *Proc. 15th Conf., IAHR*, 1, 341-352.
- STOW, D.A.V., HOWELL, D.G., and NELSON, C.H. (1985), Sedimentary, tectonic, and sea-level controls. , *Submarine Fans and Related Turbidite Systems*, edited by A.H. Bouma, W.R. Normark, and N.E. Burnes, Springer-Verlag, New York.
- TAKAHATA, S. (1995), A numerical model of turbidity currents. M.S. thesis, Dept. of Civil Eng., Univ. of Minn., Minneapolis.
- TESAKER, E. (1969), Uniform turbidity currents. Thesis in Civil Eng., Tech. Univ. of Norway, 200 p.
- TSIHRINTZIS, V.A., and ALAVIAN, V. (1996), Spreading of three-dimensional inclined gravity plumes. *J. Hyd. Res.* 34(5), 695-711.
- TURNER, J.S. (1973), *Buoyancy Effects in Fluids*. Cambridge Univ. Press, Cambridge, U.K., 367 p.
- TWICHELL, D.C., KENYON, N.H., PARSON, L.M., and MCGREGOR, B.A. (1991), Depositional patterns of the Mississippi fan surface: Evidence from GLORIA II and high-resolution seismic profiles, In: *Seismic Facies and Sedimentary Processes of Submarine Fans and Turbidite Systems*, 349-363, Paul Weimer, and Martin H. Link Eds. Springer-Verlag, New York.

#### Acknowledgments

This research was supported by the National Science Foundation (grants CTS-9207882 and CTS- 9424507) and the STRATAFORM Program of the Office of Naval Research. Jeff Marr participated in building the experimental setup. The manuscript benefited from reviews by two anonymous reviewers.